

PyroFocus: A Deep Learning Approach to Real-Time Wildfire Detection in Multispectral Remote Sensing Imagery

Mark Moussa, Andre Williams, Seth Roffe, Douglas Morton
NASA Goddard Space Flight Center

{mark.m.moussa, andreali.williams, seth.roffe, douglas.morton}@nasa.gov

Abstract

Rapid and accurate wildfire detection and quantification are crucial for emergency response and environmental management. In airborne and spaceborne missions, it is useful for real-time detection algorithms to not only classify whether the observed area consists of no fire, active fire or post-fire, but also to discriminate among varying fire intensities. Hyperspectral and multispectral thermal imagers provide sufficient spectral information to address these challenges; however, high data dimensionality and limited onboard resources complicate real-time processing. With wildfires becoming more common, the need for real-time detection is crucial for successful wildfire management and damage mitigation. It is therefore imperative for onboard solutions to achieve both high accuracy and low inference latency at minimal computational cost.

*In this work, we present several contributions divided into two main parts. First, we systematically evaluate multiple cutting-edge deep learning architectures, such as custom Convolutional Neural Networks (CNN) and Transformer-based models for multi-class fire classification. Second, we propose a novel adaptation of a two-stage pipeline, which we call **PyroFocus**, consisting of classification of fires and fire radiative power (FRP) regression or image segmentation, designed to significantly reduce inference times and computational requirements for onboard wildfire detection in airborne and spaceborne applications. We evaluate model accuracy, inference latency, and computational cost to identify the most effective solution for resource-constrained environments. Our study leverages a dataset from NASA's MODIS/ASTER Airborne Simulator (MASTER), which provides data similar to that of an in-house next-generation fire detection sensor; NASA's Compact Fire Imager (CFI) [19].*

Experimental results indicate that the proposed two-stage pipeline provides favorable trade-offs among inference speed and accuracy, demonstrating strong potential for edge deployment in future wildfire monitoring missions.

1. Introduction

Wildfires rank among the most destructive and rapidly evolving natural disasters, posing severe threats to ecosystems, human lives, and infrastructure. Early detection and precise quantification of wildfire intensity can critically enhance emergency response efforts and resource allocation. Airborne and spaceborne sensor systems, which provide broad geographic coverage at various revisit frequencies, have emerged as vital tools in monitoring wildfires. However, the operational limitations of space platforms, such as slow downlink speeds and resource-constrained computing systems, still act as a barrier for real-time data processing and detection. These barriers can be overcome with the advent of onboard data processing, where algorithms onboard the spacecraft provide the majority of any analysis processing prior to downlink.

Recent advances in artificial intelligence and machine learning (AI/ML), and in particular, deep learning, have shown promise for extracting complex spectral-spatial features from hyperspectral and multispectral data [28]. However, the high dimensionality and data sizes of these imagery and the necessity for low-latency inference highlight the need for specialized architectures and model pipelines. Furthermore, these deep learning architectures tend to use significant computational resources, which may not be problematic in most cases, but can prove troublesome when dealing with deployment on a heavily resource-constrained system. Balancing accuracy with computational efficiency remains an open challenge.

One of the key methods for characterizing wildfires is Fire Radiative Power (FRP), a well-established metric linked to energy release rates. Accurate FRP estimation can provide further insight into the wildfire dynamics beyond metrics linked to the location and duration of fire activity, such as fire intensity and radiant heat. FRP offers valuable insights into fire behavior, spread potential, and severity. High FRP values indicate intense fires likely to grow rapidly [14], and thus quantifying FRP can support resource allocation for suppression efforts. Additionally, FRP plays a key

role in estimating biomass combustion rates and associated carbon emissions [15], supporting studies on air quality and climate impact. In order to provide responsive and precise wildfire management and damage mitigation, these predictive metrics become critical. Therefore, real-time onboard sensor processing needs to keep up with desired response time by providing these metrics with careful attention to inference speed and model efficiency.

In this paper, we tackle these inference latency challenges in two ways: first, we perform a comprehensive evaluation of CNN and Transformer models for multi-class wildfire classification. For this, we elect to focus mainly on model accuracy, since accuracy is ultimately the most important metric when it comes to the detection of wildfires; false positives or false negatives can both have penalizing effects in downstream wildfire mitigation operations. We then utilize the best classification model and compare alongside two distinct strategies for FRP regression: a traditional approach, where we perform regression over every pixel, regardless of whether the patch contains a fire or not, versus PyroFocus, our two-stage pipeline that first classifies fire pixels and then estimates their radiative power. By separating classification from regression, the PyroFocus approach has the potential to significantly reduce the workload, since only the fire-labeled regions require the more computationally expensive FRP analysis. We conduct experiments using data from NASA’s MODIS/ASTER Airborne Simulator (MASTER) [9], selecting nine specific bands to mirror the capabilities of an in-house sensor under development, NASA’s Compact Fire Imager (CFI). We benchmark the approaches with respect to accuracy, inference speed, and computational cost, shedding light on the trade-offs inherent in different architectures and pipeline designs.

2. Related Works

Deep learning has become a powerful tool in remote sensing, advancing tasks such as classification, segmentation, and regression on multispectral and hyperspectral data [1, 6]. Convolutional Neural Networks have proven effective for extracting complex spectral–spatial features, while Transformer-based models leverage attention mechanisms for potentially improved accuracy. However, these deep models often demand significant computational resources, posing challenges for onboard or real-time processing in resource-constrained environments.

In wildfire detection specifically, specialized frameworks such as Fire-Net show that integrating optical and thermal data can achieve high accuracy, even for small fires [23]. Similar AI-driven systems have also demonstrated rapid alert generation capabilities in severe events like the Australian wildfires [24]. Comprehensive reviews highlight the versatility of ML methods for broader wildfire science, cov-

ering tasks such as fuel characterization, mapping, weather analysis, and fire behavior prediction [11]. Yet these studies also underscore key limitations: balancing accuracy with inference speed, handling class imbalance, and confronting hardware constraints remain open challenges. Recent advancements in early wildfire detection from hyperspectral satellite images [25] and reviews of deep learning methods for forest fire surveillance systems [21] further emphasize these challenges. This work builds on these insights by proposing a two-stage pipeline that emphasizes both accuracy and resource efficiency for real-time wildfire detection and FRP estimation.

3. Methods

This section describes the processes used to achieve two main objectives: evaluating several model performances for the multi-class classification of fire images, and evaluating the efficacy of our proposed two-stage model pipeline (PyroFocus) vs. a traditional one-stage model pipeline.

3.1. Dataset

3.1.1. Data source

We utilized data coming from the MASTER 2019 campaign. Specifically, we used the data collected from the Fire Influence on Regional to Global Environments and Air Quality (FIREX-AQ) program, which consists of 21 flights spanning from July to September 2019. We used this dataset specifically because some of the bands provided are similar in nature to CFI, a sensor currently being developed in-house at NASA Goddard Space Flight Center [19]. The MASTER sensor collects multispectral imagery, consisting of 50 bands, covering wavelengths of 0.460 to 12.879 micrometers at varying spatial resolution. The spectral information collected is similar to that provided by the Moderate Resolution Imaging Spectroradiometer (MODIS) onboard Terra and the Advanced Spaceborne Thermal Emission and Reflection Radiometer (ASTER) onboard Terra and Aqua [9].

3.1.2. Band selection

For our use case, we selected nine of the 50 spectral bands available from the MASTER dataset. The motivation of selecting these bands in particular was not only to closely resemble the data for NASA’s CFI, but also to pick the bands best-suited for wildfire detection. We selected bands from the shortwave infrared (SWIR) wavelength, the mid-wave infrared (MWIR) and the long-wave infrared (LWIR) regions. SWIR bands are primarily used here for detecting reflected solar radiation, but these wavelengths are also useful for identifying emitted radiation from hot fires. MWIR and LWIR regions constitute the thermal infrared (TIR) range. MWIR is commonly used in fire detection because it captures the peak emission from high-temperature sources

(e.g., flaming fires), while LWIR is useful for capturing smoldering fires, and for background temperature differentiation. Thus, these selected bands are well-suited to detect various aspects of wildfires. Table 1 shows the specific bands selected.

Wavelength Region	Spectral Bands (μm)
Shortwave Infrared (SWIR)	2.160, 2.210, 2.260
Midwave Infrared (MWIR)	3.755, 3.910
Longwave Infrared (LWIR)	8.200, 11.330, 12.130

Table 1. Grouping of selected spectral bands from the MASTER sensor into wavelength regions.

3.1.3. Preprocessing

Our data pipeline processes MASTER sensor data stored in Hierarchical Data Format (HDF) files to create analysis-ready datasets. The workflow begins by selecting a subset of HDF files from our multispectral imagery collection. Then, in our preprocessing pipeline, we begin by extracting calibrated spectral measurements and applying radiometric calibration using instrument-specific scale factors. Next, we extract precise geographic coordinates for each pixel to enable accurate geolocation. The resulting 3D data array (height \times width \times bands) is then converted into a GeoPandas format with wavelength-based column names, ensuring that the data is spatially co-located and well-organized so that the ML training process can effectively leverage spatial features. For FRP estimation, we associate each FRP value with its corresponding pixel by employing a nearest-neighbor spatial join with a 5-meter threshold. Finally, the data is converted back from GeoPandas to NumPy matrices to facilitate faster data-loading performance. This process is only done once, when initially preprocessing the dataset. The resulting dataset is saved out to disk, which will then be used for training, validation, and testing.

The next step we took was implementing a patch-based processing strategy. Each patch has dimensions $H \times W \times C$, where H and W represent the height and width of the patch in pixels, and C is the number of spectral bands used (spectral bands can be found in Table 1). In our case, we set $H = 24$, $W = 64$, and $C = 9$. Using image patches for training allows for efficient representation of spatially rare events such as fires, facilitates balanced sampling between fire and non-fire classes, and improves overall data coverage. Additionally, patches enhance training via improved sampling of rare events and help maintain a balanced dataset, collectively leading to improved model performance.

In order to prepare the dataset for training and testing, a number of steps were taken. As with most ML data pipelines, data was split into training (80%), valida-

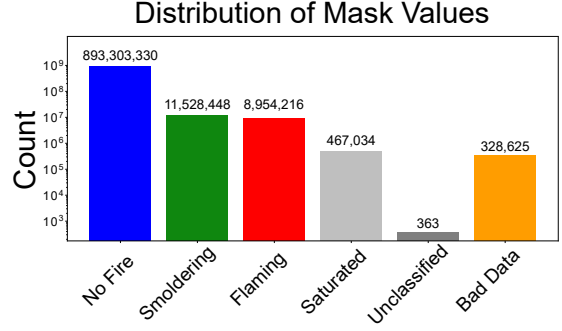


Figure 1. The distribution of pixels in our classification mask for our whole dataset, before data augmentation. The No Fire class contains orders of magnitude more pixels than any other class in the distribution (note the logarithmic scale on the y-axis).

tion (10%), and testing (10%) splits. A scaler was fit on the training data only, and used on the training, validation, and test set. This ensures consistent data transformations across all splits, prevents data leakage, and improves model stability by scaling input features [12]. Three scaling methods—MinMax, Standard, and Robust—were tested. MinMax was chosen as it yielded slightly better performance.

Due to the significant class imbalance between *No Fire* pixels and those belonging to *Fire*, *Smoldering*, and *Saturated* classes, dataset augmentation was applied to the training set. This augmentation involved horizontally or vertically flipping and adding Gaussian noise exclusively to patches known to contain fire, smoldering, or saturated pixels. By patching the images beforehand, we ensured a more balanced split between *No Fire* and the combined fire-related classes, by selectively augmenting only regions containing fire or smoldering pixels. This approach reduced redundant augmentations of non-fire areas. Figure 1 depicts the class distribution before augmentation.

3.2. Classification

A crucial initial step is rapidly determining if a patch contains active fire and characterizing its intensity. We formulate this as a four-class classification: *No Fire* (no thermal anomaly), *Smoldering* (moderate thermal signatures, typical of lower-temperature combustion, often found at the edges of the fire or in residual combustion areas), *Flaming* (strong mid-wave infrared anomalies indicative of active burning fronts), and *Saturated* (pixels exceeding sensor limits due to extreme fire intensity or sensor limitations). This coarse classification quickly filters large satellite images, minimizing computational overhead for subsequent, more expensive pixel-level segmentation or FRP prediction.

First, we employed a custom lightweight 2D CNN optimized for small input dimensions. Additionally, we evaluated deeper and shallower ResNet variants, ultimately de-

ciding on a lightweight ResNet-18, adapted specifically for multi-band data [7]. We further explored promising approaches from recent literature, such as MobileNetV3, which employs depthwise separable convolutions and efficient bottleneck structures to factorize standard convolutions into smaller, more efficient matrix multiplications. This factorization substantially reduces computational complexity and memory requirements, making MobileNetV3 particularly suitable for onboard deployment in resource-constrained environments [10]. Finally, we evaluated the Spectral-Spatial Residual Network (SSRN), a specialized architecture that leverages residual connections to effectively capture subtle spectral-spatial relationships inherent in hyperspectral and multispectral imagery, enhancing the model’s capability to discriminate fine-grained features [4]. For MobileNetV3 and SSRN, we utilized the same architectures described in their respective papers (for MobileNetV3 we use the “MobileNetV3-Small,” configuration), and made required modifications for our input layers.

To take advantage of global or long-range context in our data, we further experimented with Vision Transformers (ViT) [5]. In our ViT implementation, each patch is subdivided into smaller blocks of 6×8 (height \times width) in the spatial dimensions and projected into embedding vectors that incorporate the spatial and spectral dimensions. We embed these vectors with positional encodings so that the transformer’s self-attention mechanism can learn both spatial and spectral relationships. The final output from the transformer encoder is then passed to a classification head.

In preliminary experiments, we also evaluated additional models, including MaskedSST [22], Hybrid CNN Transformer, and classical tree-based machine learning baselines (Random Forest [2] and XGBoost [3]). However, these approaches consistently underperformed compared to the selected models, likely due to small dataset size or the niche datatype of hyperspectral imagery. For conciseness and to maintain focus on the most promising methods with the lowest latency possibility, their detailed results have been excluded from the main discussion.

All of our models were trained using cross-entropy loss, over 30 epochs, a batch size of 128 patches, and with a learning rate of 0.001. These hyperparameters were chosen by performing a grid search, and were found to yield the best results. We used various activation functions across inner layers and architectures, such as Rectified Linear Unit (ReLU) [18], Leaky ReLU [17], Gaussian Error Linear Unit (GELU) [8], and H-swish [10]. For all of our models, we used the Adam optimizer [13]. While, due to space constraints, detailed descriptions of the evaluated model architectures are omitted here, we plan to make these details available through an open-source implementation in the near future.

3.3. Regression and Segmentation

The regression approach quantifies fire intensity by predicting FRP values for each pixel in multispectral imagery, while the segmentation task assigns a categorical label of *No Fire*, *Smoldering*, *Flaming*, or *Saturated* to each pixel, offering greater nuance than binary detection. After experimenting with various model architectures, we found that a U-Net-style network consistently performed best [20]. We therefore use U-Net as the underlying model.

We use these models to compare two inference pipelines: a traditional single-stage pipeline that processes all pixels without filtering, and the PyroFocus pipeline, which first applies a lightweight classifier to identify likely fire-containing patches before forwarding them to specialized U-Net models for detailed segmentation or FRP regression.

For FRP regression, we employ a Residual U-Net that replaces standard convolution blocks with residual blocks. Each residual block consists of two convolutional layers, batch normalization, ReLU activation, and a skip connection that helps preserve gradients during training. The network’s encoder path uses max pooling to reduce spatial dimensions, and the decoder path upscales via transposed convolutions. We also include deep supervision at multiple scales to encourage better feature learning. A custom loss combines masked mean absolute error (MAE) for focusing on fire pixels, mean squared error (MSE) for handling larger FRP values, and a false positive penalty for discouraging predictions in no-fire areas.

For pixel-wise fire segmentation, we adapt the same Residual U-Net backbone, replacing the final regression layer with a multi-class softmax head trained via cross-entropy. The core encoder-decoder structure and skip connections remain unchanged from the FRP version. We trained these models over 30 epochs, with a batch size of 32 patches, inner layer activations of ReLU, and an Adam optimizer with a learning rate of 0.001.

4. Results

In this section, we present and discuss the results of our experiments. This will be split up by task, namely the multi-class classification results, the segmentation results, and the FRP regression results.

For sections 4.2 and 4.3, inference time comparisons were conducted on the ten images from the test set with the highest fire activity, ensuring that the reported inference times for the second stage reflect the maximum expected runtime across the entire test set. This work was evaluated using a 32GB NVIDIA Tesla V100 GPU.

4.1. Classification

Figure 2 shows the overall accuracy achieved by each model (Spectral Former, MobileNetV3, Vision Trans-

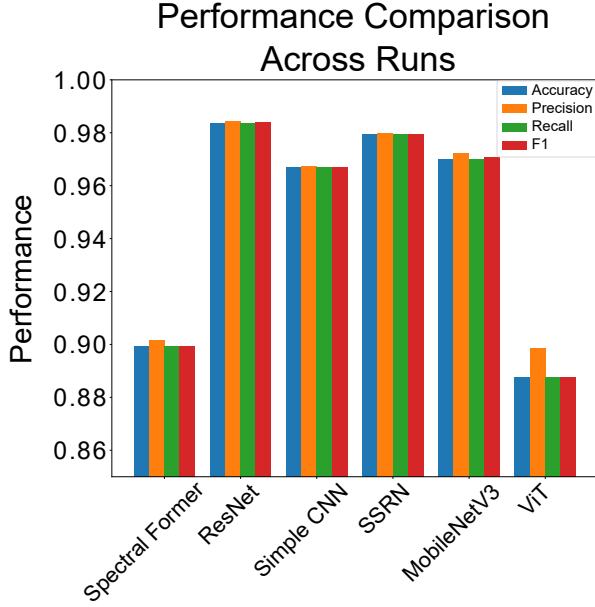


Figure 2. Bar charts comparing accuracy, precision, recall, and F1 score across all models.

former, ResNet, SSRN, and Simple CNN).

The normalized confusion matrices for each model are presented in Figure 3. Each sub-figure highlights the distribution of predictions across the four classes (*No Fire*, *Smoldering*, *Flaming*, and *Saturated*). The diagonal elements of these matrices illustrate each model’s ability to correctly classify samples of a given class, whereas off-diagonal cells indicate misclassifications.

Run Name	Inference Time (ms)	Total Parameters (M)
Spectral Former	3.31	21.1
ResNet	1.51	6.7
Simple CNN	0.48	1.77
SSRN	1.01	0.25
MobileNetV3	4.37	6.86
Vision Transformer	3.16	27.7

Table 2. Inference time (in milliseconds) and total parameters (in millions) for various models. Tested on a Tesla V100 GPU.

Finally, Table 2 summarizes each model’s inference time and total parameters.

Considering accuracy, precision, recall, and F1-scores (Figure 2), confusion matrices (Figure 3), and computational efficiency (Table 2), ResNet emerges as the best overall choice, offering an optimal balance between high classification performance across all fire intensity categories and relatively fast inference time. SSRN also demonstrates strong accuracy with even fewer parameters and lower la-

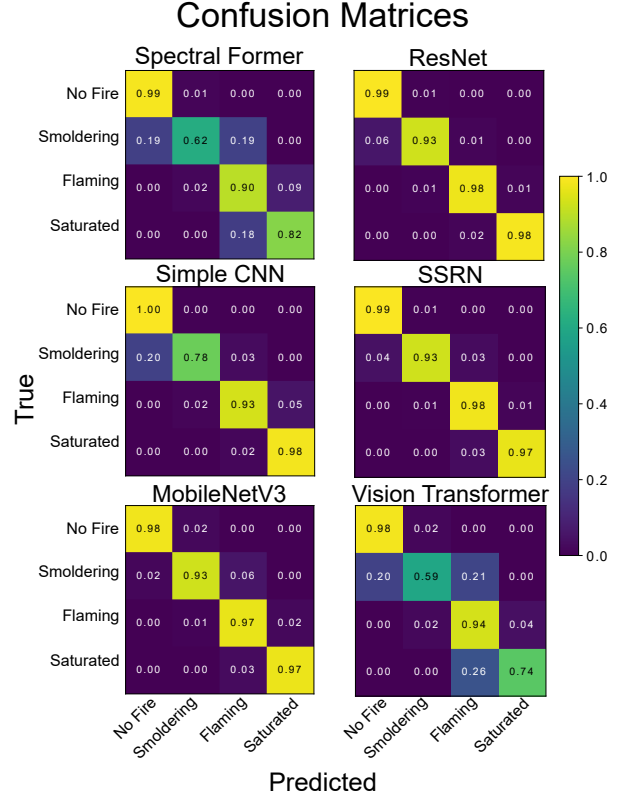


Figure 3. Normalized confusion matrices for each model. Each cell shows the fraction of predictions for a given class (row) classified into each predicted category (column).

tency, making it highly suitable for extremely resource-constrained scenarios, whereas MobileNetV3, despite good accuracy, incurs significantly higher computational cost. By contrast, Spectral Former and Vision Transformer show inferior intermediate-class performance coupled with higher inference times and parameter counts, limiting their suitability for onboard deployment.

4.2. FRP Regression

Our FRP regression experiments compared the traditional method of a single end-to-end U-Net with our PyroFocus method, which uses two stages to first implicitly mask non-fire pixels, so that the second stage, in this case the U-Net, focuses solely on confirmed fire pixels. As shown in Figure 5, the traditional end-to-end model generally tracked observed FRP distributions but occasionally produced negative predictions in no-fire areas, suggesting overfitting in regions lacking thermal anomalies.

Figure 6 shows that the PyroFocus method reduced inference latency by 1.07 seconds, or a 49.5% improvement, while maintaining comparable performance metrics (MAE = 0.00349) compared to the baseline.

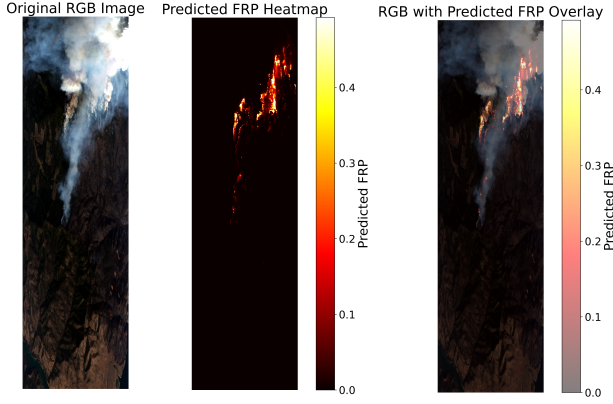


Figure 4. Comparison of an original RGB image of an active wildfire (left), the model's predicted FRP heatmap (center), and the overlay of the predicted FRP on the RGB image (right). FRP is in MW.

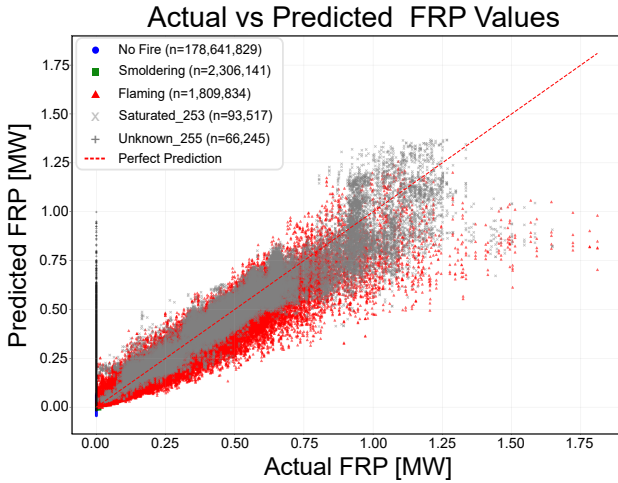


Figure 5. Actual vs. predicted values of pixels for FRP prediction.

4.3. Segmentation

Figure 6 shows that the PyroFocus segmentation approach reduced inference time by an average of 1.989 seconds, or a 73.6% improvement, compared to the traditional single-stage baseline. In terms of pixel-wise accuracy, both methods correctly identified major clusters of high-intensity pixels (*Flaming* and *Saturated*) and low-intensity regions (*No Fire* and *Smoldering*) at similar rates, but the PyroFocus method processed fewer total pixels and completed segmentation significantly faster. In test samples with partially saturated regions, both models occasionally misassigned some boundary pixels, though overall metrics suggest comparable robustness between the traditional and PyroFocus methods.

Fire-Net [23] was also trained on the MASTER dataset to compare PyroFocus with the current state-of-the-art. Table 3 reports inference time (batch size = 64) and mean IoU.

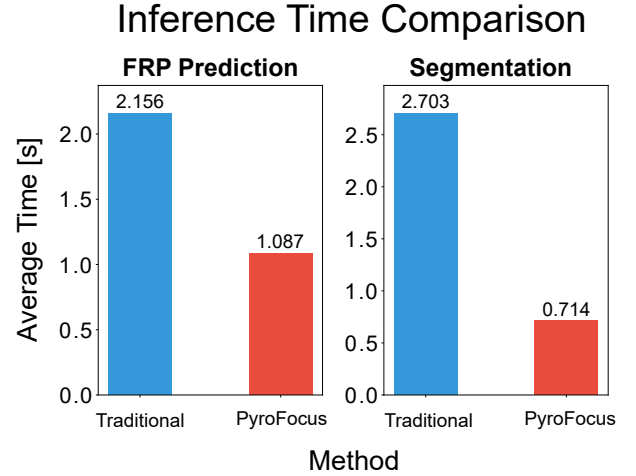


Figure 6. Inference time (in seconds) comparison between the single end-to-end FRP regression and PyroFocus method of FRP regression (left), and the single end-to-end segmentation and PyroFocus method of segmentation (right).

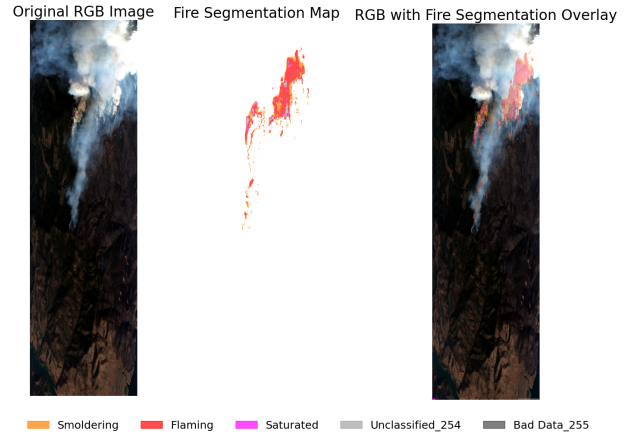


Figure 7. Comparison of an original RGB image of an active wildfire (left), the model's predicted segmentation mask (center), and the overlay of the segmentation mask on the RGB image (right).

Method	MIoU	Inference Time [s]
Fire-Net	0.9222	2.53
PyroFocus	0.9916	0.71

Table 3. Inference Times and IoU Model Comparisons.

5. Discussion

The primary aim of this work was to explore deep-learning-based approaches for onboard wildfire detection and characterization in resource-constrained environments by leveraging multispectral data from NASA's MASTER sensor. This section interprets our results and highlights the

implications, limitations, and broader insights.

5.1. Multi-Class Classification

Our multi-class classification framework targeted four distinct categories (*No Fire*, *Smoldering*, *Flaming*, and *Saturated*) to capture a range of fire intensities without resorting to a simple binary split. Through most of the model architectures tested, several trends emerged that inform how spectral and spatial cues should be leveraged. High overall accuracies masked important nuances related to fire intensity. The confusion matrices in Figure 3 show that most models easily distinguished between no-fire patches and heavily flaming or fully saturated regions, where the thermal signals are unmistakably strong. Smoldering patches posed greater difficulty, often leading to confusion with either low-level flaming or non-fire areas, especially when the visible flaming boundary was not sharply defined. This could be due to subtle spectral-spatial cues that were insufficiently captured by certain architectures.

ResNet and SSRN consistently exhibited the strongest performance across the fire intensity classes, effectively minimizing misclassification errors, particularly for challenging intermediate classes such as *Smoldering* (Figures 2 and 3). SSRN in particular seems quite promising, due to its significantly reduced parameter size (0.25M parameters) and inference time (1.01 ms) (Table 2), while also incorporating an attention mechanism and achieving an accuracy of 98.4%. MobileNetV3 also performed well across these classes, although it showed slightly lower accuracy (97.0%) compared to ResNet and SSRN (Figure 2). However, the established efficiency and optimization potential of MobileNetV3’s architecture, specifically its use of depth-wise separable convolutions and efficient bottleneck structures tailored for resource-constrained edge hardware [10], remains compelling for practical onboard implementations. Future exploration through quantization, additional architectural tuning, and hardware-specific optimizations may help clarify its true performance. We believe ultimately MobileNetV3 may indeed still be the best model architecture, as the lower performance compared to ResNet and SSRN may be small enough to overcome with further development. Future research, specifically comparing these models after quantization, further architecture design considerations, and hardware-specific optimizations are needed in order to illuminate which model truly has the best onboard performance.

While ViT-based approaches retained global context effectively, Spectral Former and Vision Transformer showed more pronounced difficulties with intermediate classes, particularly with the *Smoldering* class. While Transformer-based architectures could theoretically reduce intermediate-stage misclassifications, our results indicate that smaller or specialized CNNs like ResNet, SSRN, and MobileNetV3

provided a more efficient balance between capturing necessary context and computational performance. This may be due to the nature of Transformer-based architectures requiring significantly more training data to converge properly. Thus, while utilizing more training data can be explored in the future, this can potentially produce a non-favorable trade-off by indirectly increasing the model parameter size to achieve a similar performance, which would ultimately hinder the onboard capabilities of these models.

5.2. FRP Regression

For FRP prediction, early results suggest that using the PyroFocus method, (i.e., combining classification with a follow-up regression) on only the identified fire pixels can reduce processing overhead without compromising FRP accuracy. Traditional single-stage methods (i.e., regressing on every pixel in an entire scene) unnecessarily devote computational effort to non-fire pixels, most of which remain at or near zero FRP. This leads to higher inference latency, which is an undesirable outcome for airborne or spaceborne missions with real-time constraints.

In addition, because FRP values tend to be heavily skewed as many pixels have relatively low or no fire intensity, while a small fraction saturate the sensor, FRP regression is a challenging learning target. Even slight miscalibrations can lead to large absolute errors for the small subset of very high-intensity pixels. PyroFocus mitigates this imbalance by first determining which areas legitimately need FRP estimation and then applying a regression model calibrated specifically on those fire-containing pixels. Empirically, this approach delivered robust results, most notably in its ability to handle outliers with extremely high FRP levels (Figure 5). By focusing regression solely on fire-labeled patches, PyroFocus roughly halves the inference time (Figure 6) without degrading overall performance. Further evaluation of alternative loss functions and model architectures could potentially yield additional improvements.

5.3. Segmentation

We observed similar benefits for fire segmentation as in section 5.2 by applying the PyroFocus method. A traditional end-to-end network must process all pixels, including those without thermal anomalies, which increases computation. In contrast, Figure 6 shows that PyroFocus, which localizes fires before segmentation, significantly reduces inference time by over 70% while retaining similar segmentation quality (Figure 7). The faster runtime, but similar quality in the PyroFocus approach underscores how a cascade that localizes fires first and then conducts detailed per-pixel labeling can outperform a monolithic model pipeline. Occasional confusions arose where partial saturation overlapped with truly intense fires in neighboring pixels, but notably, the consistency of *Smoldering* or *Flaming* labels improved

when each segmenting model trained on fewer irrelevant pixels. Segmentation maps capture flaming cores and smoldering edges with reduced false positives, underscoring the efficiency of a targeted two-stage pipeline for detailed fire mapping.

5.4. Limitations and Practical Considerations

Despite encouraging outcomes, there are important limitations to acknowledge. Although we leveraged data from the MASTER 2019 FIREX-AQ campaign, which covers multiple flight lines and fire events, it still represents a finite geographic and temporal scope. Fires in different ecosystems (e.g., boreal versus tropical regions) with varying fuel compositions may exhibit somewhat different spectral responses, limiting generalization. Further work incorporating different datasets is necessary to reduce bias and generalization, and is currently underway by the team.

While we identified spectral bands less prone to saturation, extremely intense fires can still produce reflectance values at or near the sensor limit. The *Saturated* class helps capture this phenomenon but does not fully remedy the challenge of losing additional information above saturation thresholds.

Finally, while using the PyroFocus method helps reduce the proportion of obvious non-fire data, during inference there are still abundant background non-fire pixels within patches that do contain fire. This can lead to over-prediction of the non-fire class at the pixel level, artificially inflating performance metrics. Consequently, overfitting on non-fire pixels still remains a concern for the second stage, and further refinement, perhaps through additional training data, will be crucial for robust generalization.

5.5. Broader Implications

The broader significance of these findings extends beyond wildfire detection alone. Our demonstrated pipelines underscore the feasibility of applying advanced deep networks for time-critical remote sensing tasks. As constellations of small satellites and airborne campaigns increase, the need for onboard intelligence that can filter, classify, and prioritize data before downlink is growing. Because our model architectures primarily rely on convolutional operations or self-attention mechanisms that operate on tokenized patch embeddings, these models can be adapted with minimal modifications to different patch sizes or entire images, allowing for greater flexibility in spatial dimensions. Moreover, applying a two-stage detection–regression paradigm could be adapted to other contexts, such as flood monitoring (e.g., identify flood pixels, then regress on water depth) or agricultural assessments (e.g., identify crop stress areas, then quantify damage severity). Our technique of targeted recognition of interesting phenomena can even be extended to the planetary science domain and beyond.

6. Future Work

Although our two-stage PyroFocus method can potentially significantly reduce onboard inference time by intelligently focusing computation on relevant regions, further optimizations remain. In particular, quantization and other edge computing techniques have proven effective at shrinking model size while preserving accuracy [16, 26]. We plan to benchmark several of these methods on devices such as the NVIDIA Jetson Orin NX. Beyond hardware-specific improvements, we also see value in refining model architectures. The parameter space of deep networks is vast, and automated searches (e.g., Network Architecture Search (NAS) [10]) and Bayesian optimization [27] can uncover new configurations that outperform our current designs. By combining these hardware and architectural advances, we aim to further enhance PyroFocus for real-time wildfire detection in increasingly resource-constrained environments.

7. Conclusion

In this work, we introduced PyroFocus, a two-stage deep learning pipeline designed to perform efficient, real-time wildfire detection and characterization on multispectral data from sensors such as NASA’s MASTER. By separating classification of fire patches from subsequent FRP regression or segmentation, our approach substantially reduces computational overhead without sacrificing accuracy. Through extensive experiments, we demonstrated that this strategy accelerates inference times while retaining accuracy, which can be crucial for onboard inference in airborne and spaceborne platforms.

Moreover, our findings highlight the advantage of leveraging targeted analyses: only regions flagged by the first-stage classifier undergo the more demanding pixel-level prediction, allowing the system to handle larger volumes of imagery under strict resource constraints. By accurately modeling FRP or segmenting fire patches, PyroFocus has the potential to not only improve response times for emergency management, but it also lays the groundwork for robust, fine-grained fire characterization that can inform broader assessments of ecosystem impacts.

Although the approach shows promise across multiple fire regimes, future research should expand the dataset to incorporate geographically and ecologically diverse fire events, further test different model architectures and training techniques, and integrate advanced hardware optimizations (e.g., quantization) to improve model deployment.

Ultimately, PyroFocus offers a flexible, resource-conscious framework that can be adapted for various real-time remote sensing tasks, thus enabling fast and accurate onboard data processing crucial for more responsive wildfire mitigation efforts and beyond.

References

- [1] Yakoub Bazi, Laila Bashmal, Mohamad M Al Rahhal, Reham Al Dayil, and Naif Al Ajan. Vision transformers for remote sensing image classification. *Remote Sensing*, 13(3): 516, 2021. [2](#)
- [2] Leo Breiman. Random forests. *Machine learning*, 45:5–32, 2001. [4](#)
- [3] Tianqi Chen and Carlos Guestrin. Xgboost: A scalable tree boosting system. In *Proceedings of the 22nd acm sigkdd international conference on knowledge discovery and data mining*, pages 785–794, 2016. [4](#)
- [4] Wenjing Chen, Xiangtao Zheng, and Xiaoqiang Lu. Hyperspectral image super-resolution with self-supervised spectral-spatial residual network. *Remote Sensing*, 13(7), 2021. [4](#)
- [5] Alexey Dosovitskiy, Lucas Beyer, Alexander Kolesnikov, Dirk Weissenborn, Xiaohua Zhai, Thomas Unterthiner, Mostafa Dehghani, Matthias Minderer, Georg Heigold, Sylvain Gelly, et al. An image is worth 16x16 words: Transformers for image recognition at scale. *arXiv preprint arXiv:2010.11929*, 2020. [4](#)
- [6] Evan W Gretok and Alan D George. Onboard multi-scale tile classification for satellites and other spacecraft. In *2021 IEEE Space Computing Conference (SCC)*, pages 110–121. IEEE, 2021. [2](#)
- [7] Kaiming He, Xiangyu Zhang, Shaoqing Ren, and Jian Sun. Deep residual learning for image recognition. In *Proceedings of the IEEE conference on computer vision and pattern recognition*, pages 770–778, 2016. [4](#)
- [8] Dan Hendrycks and Kevin Gimpel. Gaussian error linear units (gelus). *arXiv preprint arXiv:1606.08415*, 2016. [4](#)
- [9] S.J. Hook, J.S. Myers, K.J. Thome, M. Fitzgerald, A.B. Kahle, Airborne Sensor Facility NASA Ames Research Center, J.H. Crawford, C. Warneke, and J.P. Schwarz. Master: Firex-aq airborne campaign, western-central usa, summer 2019, 2021. [2](#)
- [10] Andrew Howard, Mark Sandler, Grace Chu, Liang-Chieh Chen, Bo Chen, Mingxing Tan, Weijun Wang, Yukun Zhu, Ruoming Pang, Vijay Vasudevan, et al. Searching for mobilenetv3. In *Proceedings of the IEEE/CVF international conference on computer vision*, pages 1314–1324, 2019. [4](#), [7](#), [8](#)
- [11] Piyush Jain, Sean C.P. Coogan, Sriram Ganapathi Subramanian, Mark Crowley, Steve Taylor, and Mike D. Flannigan. A review of machine learning applications in wildfire science and management. *Environmental Reviews*, 28(4):478–505, 2020. [2](#)
- [12] Harpreet Kaur and Vandana Kumari. Effect of data scaling methods on machine learning algorithms and model performance. *Technologies*, 9(3):52, 2021. [3](#)
- [13] Diederik P Kingma and Jimmy Ba. Adam: A method for stochastic optimization. *arXiv preprint arXiv:1412.6980*, 2014. [4](#)
- [14] Pierre Laurent, Florent Mouillot, M. Vanesa Moreno, Chao Yue, and Philippe Ciais. Varying relationships between fire radiative power and fire size at a global scale. *Biogeosciences*, 16:275–288, 2019. [1](#)
- [15] Fangjun Li, Xiaoyang Zhang, Shobha Kondragunta, and David P. Roy. Investigation of the fire radiative energy biomass combustion coefficient: A comparison of polar and geostationary satellite retrievals over the conterminous united states. *Journal of Geophysical Research: Biogeosciences*, 123(2):722–739, 2018. [2](#)
- [16] Zhenhua Liu, Yunhe Wang, Kai Han, Wei Zhang, Siwei Ma, and Wen Gao. Post-training quantization for vision transformer. In *Advances in Neural Information Processing Systems*, pages 28092–28103. Curran Associates, Inc., 2021. [8](#)
- [17] Andrew L Maas, Awni Y Hannun, and Andrew Y Ng. Rectifier nonlinearities improve neural network acoustic models. In *Proc. icml*, 2013. [4](#)
- [18] Vinod Nair and Geoffrey E Hinton. Rectified linear units improve restricted boltzmann machines. In *Proceedings of the 27th International Conference on Machine Learning (ICML-10)*, pages 807–814, 2010. [4](#)
- [19] NASA Earth Science and Technology Office. Cfi: The airborne compact fire imager, 2025. Accessed: 2025-03-03. [1](#), [2](#)
- [20] Olaf Ronneberger, Philipp Fischer, and Thomas Brox. U-net: Convolutional networks for biomedical image segmentation. In *Medical image computing and computer-assisted intervention—MICCAI 2015: 18th international conference, Munich, Germany, October 5-9, 2015, proceedings, part III 18*, pages 234–241. Springer, 2015. [4](#)
- [21] Azlan Saleh, Mohd Asyraf Zulkifley, Hazimah Haspi Harun, Francis Gaudreault, Ian Davison, and Martin Spraggon. Forest fire surveillance systems: A review of deep learning methods. *Heliyon*, 10(1):e23127, 2024. [2](#)
- [22] Linus Scheibenreif, Michael Mommert, and Damian Borth. Masked vision transformers for hyperspectral image classification. In *Proceedings of the IEEE/CVF Conference on Computer Vision and Pattern Recognition (CVPR) Workshops*, pages 2166–2176, 2023. [4](#)
- [23] S. T. Seydi, V. Saeidi, B. Kalantar, N. Ueda, and A. A. Halin. Fire-net: A deep learning framework for active forest fire detection. *Journal of Sensors*, 2022:8044390, 2022. [2](#), [6](#)
- [24] Kathiravan Thangavel, Dario Spiller, Roberto Sabatini, Stefania Amici, Sarathchandrakumar Thottuchirayil Sasidharan, Haytham Fayek, and Pier Marzocca. Autonomous satellite wildfire detection using hyperspectral imagery and neural networks: A case study on australian wildfire. *Remote Sensing*, 15(3), 2023. [2](#)
- [25] Nguyen Thanh Toan, Phan Thanh Cong, Nguyen Quoc Viet Hung, and Jun Jo. A deep learning approach for early wildfire detection from hyperspectral satellite images. In *Proceedings of the 7th International Conference on Robot Intelligence Technology and Applications (RiTA)*, pages 38–45, 2019. [2](#)
- [26] Jiaxiang Wu, Cong Leng, Yuhang Wang, Qinghao Hu, and Jian Cheng. Quantized convolutional neural networks for mobile devices. In *Proceedings of the IEEE Conference on Computer Vision and Pattern Recognition (CVPR)*, 2016. [8](#)
- [27] Jia Wu, Xiu-Yun Chen, Hao Zhang, Li-Dong Xiong, Hang Lei, and Si-Hao Deng. Hyperparameter optimization for machine learning models based on bayesian optimization.

Journal of Electronic Science and Technology, 17(1):26–40, 2019. [8](#)

- [28] Xiaofei Yang, Yunming Ye, Xutao Li, Raymond YK Lau, Xiaofeng Zhang, and Xiaohui Huang. Hyperspectral image classification with deep learning models. *IEEE Transactions on Geoscience and Remote Sensing*, 56(9):5408–5423, 2018.